Int. J. High Technology Ceramics **4** (1988) 281–288

14

Measurement of Transient and Stationary Creep of HPSN in Bending

T. Fett[a] & D. Munz[a,b]

[a] Kernforschungszentrum Karlsruhe, Institut für Material- und Festkörperforschung IV. [b] Universität Karlsruhe, Institut für Zuverlässigkeit und Schadenskunde im Maschinenbau, Postfach 3640, D7500 Karlsruhe 1, FRG

1 INTRODUCTION

This paper shows how the time-dependent stress–strain state of a bending bar in creep can be obtained from global deflection measurements. One major problem in creep under 4-point bending is the determination of the correct creep strains in the inner roller span from displacement measurements.

2 CREEP MEASUREMENTS

2.1 Conventional measurements

In the earlier literature, these deflections had to be determined *indirectly* from the displacement at mid-length of the testpiece or from displacements of the loading rollers. In the literature on creep measurements one will often find a very simple displacement measurement where only the deflection in the centre of the inner span is measured against a reference level, as shown by Shetty & Gordon (1979) and Grathwohl (1984).

Evaluation of the displacement measurements poses some problems. A purely elastic relation is often applied in the form

$$\varepsilon_{\max} = \frac{4h}{s^2}\left[\frac{3s^2}{2L^2 + 2Ls - s^2}\right]\delta_c \tag{1}$$

where h is the height of the bending bar, L is the outer span, s is the inner

Int. J. High Technology Ceramics 0267-3762/88/$03·50

span, and δ_c is the displacement of the centre point relative to the reference plane. This, of course, is sufficiently correct only for low creep strains.

The *creep compliance* method developed by Fluegge (1967) and Hollenberg *et al.* (1971) is based on deflections measured at the inner load points. The results obtained for the stationary creep range are: for the outer fibre stress,

$$\sigma_{max} = \frac{3(L-s)P}{bh^2}\frac{(2m+1)}{3m} \tag{2}$$

and for the outer fibre strain,

$$\varepsilon_{max} = \frac{2h(m+2)}{(L-s)(L+s(m+1))}\delta_L \tag{3}$$

Here, P is the load applied and δ_L is the displacement of the inner rollers relative to the outer one, and m is the exponent of the Norton creep law. Although it has been indicated in the literature that the creep compliance method should be restricted to the stationary creep range, eqns (2) and (3) are often wrongly applied to the whole creep test.

With the 'constitutive law',

$$\varepsilon(t, \leftarrow \sigma) = \sigma^m J(t)$$

taken as the basis for deriving eqns (2) and (3), any elastic part, $\sim \sigma/E$(E = Young's modulus), is completely ignored. These equations must therefore fall outside the stationary creep range. No stress redistribution due to creep effects can be calculated.

2.2 Direct displacement measurements

For direct displacement measurements in the inner roller span, a special test arrangement was developed by Fett *et al.* (1987). This test arrangement is sketched in Fig. 1. The displacements of the specimen are transmitted by a system of three Al_2O_3-slender rods on a balance. The signal of the LVDT was recorded as a measure of the deflection δ in the inner span. These measurements are independent of roller flattening and settlement of the supporting structure, and only the bending beam part with a constant bending moment affects the result.

The outer fibre strain ε^* is given by

$$\varepsilon^* = \frac{4h}{s^2}\delta \tag{4}$$

Creep measurements of two batches of MgO-doped hot-pressed Si_3N_4 (HPSN) (NH206, Feldmühle AG, Plochingen) with a density of 3·20 g/cm^3

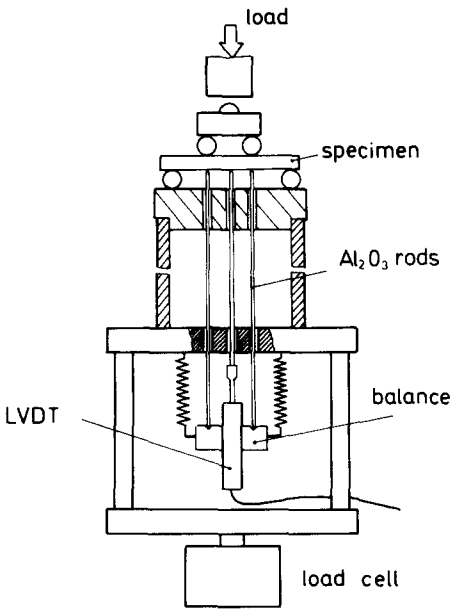

Fig. 1. Deflection measurement device.

were performed at 1300 and 1400°C. The heats were designated 'heat I' and 'heat II'. Testpieces (3·5 mm × 4·5 mm × 45 mm) were diamond-machined from plain parallel billets. The outer and inner spans of the 4-point bending arrangement were 40 mm and 20 mm, respectively. Figure 2 represents three curves obtained for heat II at 1300°C. Pronounced primary creep with very high outer fibre strain rates was encountered immediately after load application. Afterwards, the creep rates were almost constant, thus indicating secondary creep behaviour.

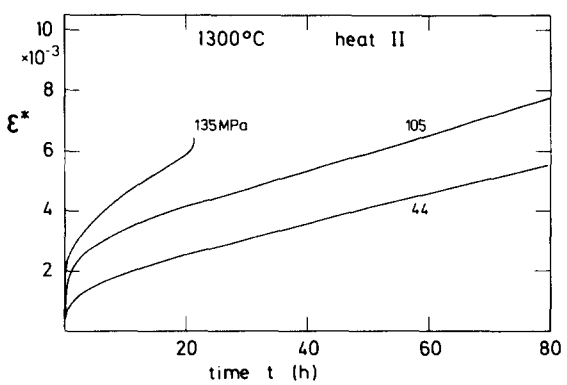

Fig. 2. Measured 'creep curves' for different initial outer fibre stresses.

3 STRESS–STRAIN BEHAVIOUR OF A CREEPING BAR UNDER BENDING

The strain rate in a fibre at the distance η from the centre axis of a bending bar of thickness h is composed of the elastic deformation rate $\dot{\sigma}/E$ and the creep rate $\dot{\varepsilon}_c$

$$\dot{\varepsilon}(y) = \dot{\sigma}(y)/E + \dot{\varepsilon}_c(y) \tag{5}$$

In agreement with Bernoulli's hypothesis, the total strain rate is linearly distributed over the specimen. One can write

$$\dot{\sigma}(y)/E + \dot{\varepsilon}_c(y) = C + \dot{\varepsilon}^* y \tag{6}$$

where $y = 2\eta/h$ is the normalised distance from the centre axis. Figure 3 shows the geometric quantities and the strain distribution in the bending bar described by eqn (6). The term C describes a change Δl in testpiece length. Only for non-symmetrical creep behaviour can $\Delta l \neq 0$ be expected to apply. The term $(\dot{\varepsilon}^* y)$ describes the typical bending behaviour resulting in the deflection δ.

By integrating eqn (6) over the cross-section, taking into account that the integral over $\dot{\sigma}$ disappears, one obtains (Fett *et al.*, 1988)

$$C = \tfrac{1}{2} \int \dot{\varepsilon}_c \, dy \tag{7}$$

Multiplying eqn (6) by y followed by repeated integration furnishes, for the constant-moment test with $\dot{M} = 0$ (M = bending moment),

$$\dot{\varepsilon}^* = \tfrac{3}{2} \int \dot{\varepsilon}_c \, y \, dy \tag{8}$$

From eqn (6), the complete stress–strain history of an arbitrarily loaded bending bar can be determined by solving the differential equation:

$$\frac{\dot{\sigma}}{E} = -\dot{\varepsilon}_c + \frac{1}{2}\int \dot{\varepsilon}_c \, dy + \frac{3}{2} y \int \dot{\varepsilon}_c \, y \, dy \tag{9}$$

as performed by Fett *et al.* (1986, 1988).

If the creep law is known, the numerical evaluation of eqn (9) yields the complete stress–strain state of the bending bar. On the other hand, eqn (9) may be used to determine the local creep law from the global outer fibre strain measurements.

4 DETERMINATION OF THE LOCAL CREEP LAW

From the characteristic features of the measured curves, $\varepsilon^* = f(t)$, the type of appropriate local creep law can be concluded. In principle, there are two

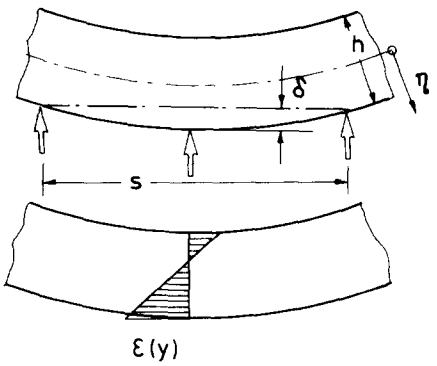

Fig. 3. Geometrical data and strain distribution.

different ways of determining the accompanying parameters. Both methods are demonstrated here. The total creep rate is seen to be composed of a primary creep rate $\dot{\varepsilon}_p$ and the secondary part $\dot{\varepsilon}_s$, such that

$$\dot{\varepsilon}_c = \dot{\varepsilon}_p + \dot{\varepsilon}_s \tag{10}$$

where, for instance,

$$\dot{\varepsilon}_p = f(\sigma, \varepsilon_p)$$

and

$$\dot{\varepsilon}_s = g(\sigma)$$

The primary creep law will be evaluated by a least-squares procedure, the secondary part by an analytical asymptotic solution of eqn (9).

4.1 Least-squares procedure

The chosen creep law of eqn (10) is substituted into eqn (9). Numerical integration of eqn (9), starting from the initial stress distribution, $\sigma_i = M/W$ (W = moment of inertia), yields $\sigma(y, t)$, $\varepsilon_p(y, t)$ and $\varepsilon^*(t)$ for any set of creep parameters. The calculated outer fibre strains can be compared with the measured ones, and minimising the expression

$$\sum[\varepsilon^*(\text{measured}) - \varepsilon^*(\text{calculated})]^2 = \text{MIN} \tag{11}$$

will furnish the best set of parameters.

In the primary creep range, extremely high outer fibre strain rates occur. This is the reason for applying Nadai's creep law (Nadai, 1938)

$$\dot{\varepsilon}_p = A\,\sigma^n\,\bar{\varepsilon}_p^{\,p} \tag{12}$$

The Harwell VA02A subroutine allowed the least-squares calculation to be performed easily. In each step of the least-squares routine, a complete set of

TABLE 1
Creep Parameters for HPSN (+MgO)

	1300°C		*1400°C*
	heat I	*heat II*	*heat I*
A (MPa,h)	$1{\cdot}35 \times 10^{-15}$	$4{\cdot}0 \times 10^{-16}$	$5{\cdot}8 \times 10^{-17}$
n	4·80	4·10	4·60
p	1·60	1·80	2·40
B (MPa, h)	$1{\cdot}45 \times 10^{-6}$	$1{\cdot}95 \times 10^{-7}$	—
m	1·75	1·75	—

20 curves $\varepsilon^*(t)$ was calculated up to $t = 0{\cdot}5$ h and compared with a set of 20 measured curves. The best parameter set A, n, p was found within two minutes of CPU time. The results are compiled in Table 1. In this procedure, only short times were taken into account to ensure that all secondary creep parts could be neglected.

4.2 Analytical solution

The secondary part $\dot{\varepsilon}_s$, often described by Norton's law, is modified to express a non-symmetrical behaviour as follows:

$$\dot{\varepsilon}_s = B \lambda_s \sigma^m \tag{13}$$

where

$$\lambda_s = \begin{cases} 1 \text{ for } \sigma > 0 \\ 1/\alpha^m \text{ for } \sigma < 0,\ \alpha \simeq 7 \end{cases}$$

where m is a constant. Equation (12) takes into consideration the significantly higher secondary creep rates than compressive stresses that occur due to tensile stresses, as described by Lange (1983). The related stationary stress distribution, as given by Fett (1986), is

$$\sigma_{(t=\infty)} = \frac{M}{W} \frac{2m+1}{3m} \left[\frac{1+\kappa}{2}\right]^{(m+1)/m} (y + y_0)^{1/m} \begin{cases} 1/\alpha & \text{for } y + y_0 > 0 \\ -1 & \text{for } y + y_0 < 0 \end{cases} \tag{14}$$

where $y = -y_0$

$$y_0 = \frac{\kappa - 1}{\kappa + 1};\ \kappa = \alpha^{m/(m+1)} \tag{15}$$

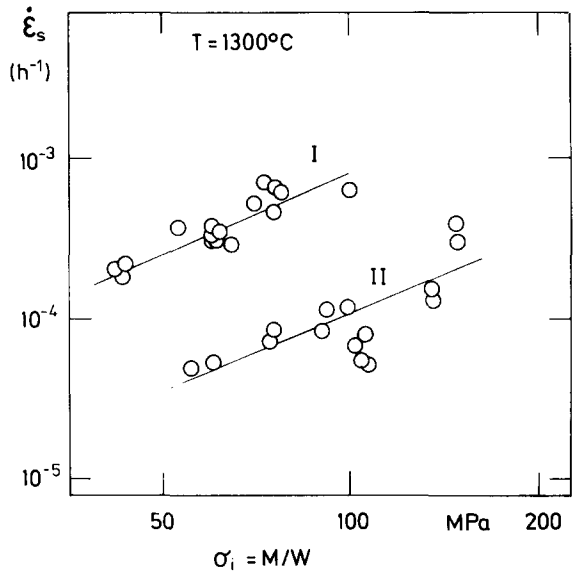

Fig. 4. Outer fibre stationary strain rates for different initial outer fibre stresses.

is the neutral fibre of the stationary stress distribution. Consequently, the strain rate on stationary outer fibre is seen to be

$$\varepsilon^*_{(t=\infty)} = \tfrac{1}{2}B\left(\frac{2m+1}{6m}\frac{M}{W}\right)^m\left(1+\frac{1}{\kappa}\right)^{m+1} \tag{16}$$

By plotting the outer fibre stationary strain rate versus the initial stress M/W, the exponent m and the coefficient B can be calculated according to eqn (16). Figure 4 shows the outer fibre stationary creep rates at 1300°C. The stationary creep data are also included in Table 1.

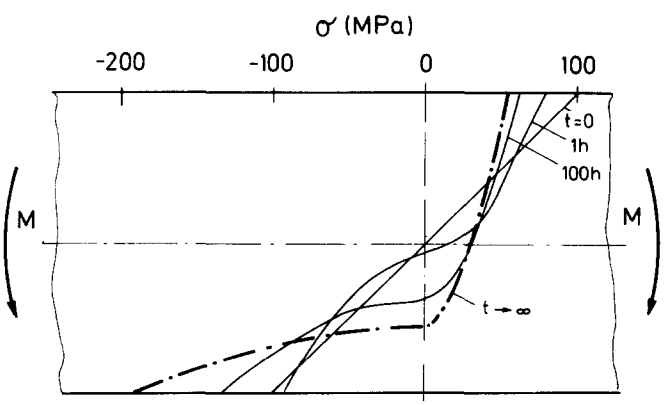

Fig. 5. Development of the stress distribution in a bending bar.

5 TIME-DEPENDENT STRESS DISTRIBUTION

As all creep parameters are known, the time-dependent stresses can be computed according to eqn (9). The result is plotted in Fig. 5. The stress development, starting from the initial linear stress distribution, is evident. The tensile stresses relax and the neutral axis is shifted into the initial compression zone.

REFERENCES

Fett, T. (1986). *Res Mechanica*, **18**, 95.
Fett, T., Himsolt, G. & Munz, D. (1986). *Advanced Ceram. Mater.*, **1**, 179.
Fett, T., Keller, K. & Rosenfelder, O. (1987). German Patent P 3629131.
Fett, T., Keller, K. & Munz, D. (1988). *J. Mater. Sci.*, **23**, 467–74.
Fluegge, W. (1967). *Viscoelasticity*, Blaisdell Publishing Co., Waltham, Mass., 1967.
Grathwohl, G. (1984). In: *Deformation of Ceramics II*, ed. R. E. Tressler & R. C. Bradt, Plenum Publishing Corp., 1984, pp. 573–85.
Hollenberg, G. W., Terwilliger, G. R. & Gordon, R. S. (1971). *J. Amer. Ceram. Soc.*, **54**, 196–9.
Lange, F. F. (1983). In *Progress in nitrogen ceramics*, ed. F. L. Riley, Martinus Nijhoff Publications, The Hague, 1983, p. 467.
Nadai, A. (1938). In *S. Timoshenko Anniversary Volume*, New York, 1938.
Shetty, D. K. & Gordon, R. S. (1979). *J. Mater. Sci.*, **14**, 2163–71.